



HAL
open science

Evaluation of sediment transport formulae and detachment parameters in eroding rills using PSEM_2D and the Water Erosion Prediction Project (WEPP) database

Guillaume Nord, Michel Esteves

► To cite this version:

Guillaume Nord, Michel Esteves. Evaluation of sediment transport formulae and detachment parameters in eroding rills using PSEM_2D and the Water Erosion Prediction Project (WEPP) database. Water Resources Research, 2007, 43, pp.W08420. 10.1029/2006WR005444 . insu-00387870

HAL Id: insu-00387870

<https://insu.hal.science/insu-00387870>

Submitted on 10 Mar 2021

HAL is a multi-disciplinary open access archive for the deposit and dissemination of scientific research documents, whether they are published or not. The documents may come from teaching and research institutions in France or abroad, or from public or private research centers.

L'archive ouverte pluridisciplinaire **HAL**, est destinée au dépôt et à la diffusion de documents scientifiques de niveau recherche, publiés ou non, émanant des établissements d'enseignement et de recherche français ou étrangers, des laboratoires publics ou privés.

Evaluation of sediment transport formulae and detachment parameters in eroding rills using PSEM_2D and the Water Erosion Prediction Project (WEPP) database

Guillaume Nord^{1,2} and Michel Esteves¹

Received 18 August 2006; revised 27 April 2007; accepted 11 May 2007; published 18 August 2007.

[1] The numerical model PSEM_2D is applied to reproduce the rill experiments described by Elliot et al. (1989) for five different textured soils. PSEM_2D is a two-dimensional water flow and erosion model incorporating the first-order detachment-transport coupling model. The infiltration parameters and the friction factor are calibrated to reproduce both the flow discharges and the flow velocities measured by Elliot et al. (1989). Values of the determined friction factors are higher for the cohesive soils compared to the noncohesive soils. Four sediment transport capacity formulae for rills are tested: the Yalin, the Low, the unit stream power (Govers USP), and the effective stream power (Govers ESP) equations. These equations do not require any calibration. The erosion parameters for the first-order detachment-transport coupling model come from the Water Erosion Prediction Project (WEPP) database. They were calibrated by Elliot et al. (1989) using observed data and the rill component of WEPP. The Govers USP formula gives the best results for the cohesive soils. Nevertheless, none of the equations performs well for the noncohesive soils. The study also focuses on the results obtained for the Barnes_ND, the Bonifay, and the Collamer soils to explore the implication of the detachment-transport coupling model on the spatial erosion patterns along the rills. A detachment-limiting regime is produced over the whole rill for the Barnes_ND soil, a transport-limiting regime is reached over a very short flow distance for the Bonifay soil, and a detachment-limiting regime in the upper part along with a transport-limiting regime in the lower part of the rills is experienced for the Collamer soil.

Citation: Nord, G., and M. Esteves (2007), Evaluation of sediment transport formulae and detachment parameters in eroding rills using PSEM_2D and the Water Erosion Prediction Project (WEPP) database, *Water Resour. Res.*, 43, W08420, doi:10.1029/2006WR005444.

1. Introduction

[2] Rills are important components in the total upland erosion process. They assure the transfer of sediment from the hillslope to the hydrographic network and can be a large source of sediment as well. It is well known that an important part of the sediment eroded on the hillslopes is deposited before entering into the hydrographic network. Studies involving tracing techniques [Walling, 1990; Polyakov and Nearing, 2004; Walling, 2005] have provided valuable data on the spatial and temporal dynamics of sediment delivery within a small catchment. Evaluation of the transport capacity of flow in rills and estimation of the sediment loads leaving a hillslope during a rainfall event

require some modeling of the processes involved in rills. Foster and Meyer [1972] and then Foster [1982] developed an important background for modeling the upland erosion on the basis of an explicit distinction between interrill and rill erosion and the fundamental equation of mass conservation of the eroded sediments. On the basis of these studies, Nearing et al. [1989] proposed a physically based soil erosion model, Water Erosion Prediction Project (WEPP), involving a first-order detachment-transport coupling model for the rill erosion component. Hairsine and Rose [1992] followed an alternative approach to model rill erosion. They considered that detachment and deposition were simultaneous processes, and that the sediment concentration was the result of the equilibrium between these two processes.

[3] Experimental studies allowed to develop and test the sediment transport capacity formulae. Govers [1992] undertook a thorough evaluation of sediment transport capacity formulae for overland flow using a large amount of data. These data were either derived from the literature or collected under laboratory conditions. The author tested existing formulae developed from observations in channels and alluvial rivers such as the Yalin formula (1963) and the

¹UMR 5564, Laboratoire d'Étude des Transferts en Hydrologie et Environnement, CNRS, Institut National Polytechnique de Grenoble, Institut de Recherche Pour le Développement, Université Joseph Fourier, Grenoble, France.

²Now at UMR 1572, Laboratoire des Sciences du Climat et de l'Environnement, CNRS, Commissariat à l'Énergie Atomique, Université de Versailles Saint-Quentin-en-Yvelines, Gif sur Yvette, France.

Low formula (1989). He also proposed simple empirical equations based on shear stress, unit stream power (Govers USP) and effective stream power (Govers ESP). He concluded that none of the equations yielded good predictions over the whole range of conditions tested. Nevertheless, the empirical equations developed from his data and the formula of Low showed reasonable to very good agreement with other data sets. Therefore they can be used in erosion models, more specifically for rill conditions. *Ferro* [1998] evaluated different sediment transport capacity equations for overland flow. He calibrated the sediment transport capacity relationship used in the WEPP model with the Yalin formula and Govers' empirical formula on the basis of shear stress. For each formula, *Ferro* [1998] expressed the transport coefficient of WEPP as a function of the Shields number (also called the dimensionless shear stress). He showed that the transport coefficient depends on the hydraulic conditions (small- or large-scale roughness). He mentioned that using these transport coefficient relationships is possible but requires a calibration step. He also tested Low's formula and transformed it to a stream power equation.

[4] Given the complexity of flow hydraulics and erosion processes in rills and their interactions, *Lei et al.* [1998] set up a mathematical model to simulate dynamically and spatially varied hydraulic and erosion processes in rills. The hydrodynamic equations described a one-dimensional water flow in a width-varied rill. A detachment-transport coupling model was involved to calculate the sediment source/sink term. The model introduced a feedback loop between erosion, hydraulics, and bed form. The purpose of this study was to gain a more complete understanding of the evolutionary process of rill development. It was a first attempt to develop an evolutionary model which mimics rill evolution by changing rill morphology over time and space. The results showed that hydraulic and erosion variables change very much with downslope distance causing both erosion and deposition in the same rill. The way the rills are eroded in the simulations depends largely on the model selected to describe the detachment and the transport of the sediment.

[5] Various large, process-based soil erosion models are available now. However, there have been very few attempts to validate the submodels or the key equations incorporated in them. PSEM_2D [*Nord and Esteves, 2005*] is a two-dimensional flow and erosion model accounting for morphological changes. It provides a modeling framework to test some of the equations used in large, process-based models. In the present paper, we use PSEM_2D to simulate rill erosion processes. The aims are to test the validity of four sediment transport capacity equations, explore the implications of the detachment-transport coupling concept (the validity of this coupling concept is not tested) and examine the ability of the Saint Venant equations to represent eroding rills.

2. Materials and Methods

[6] The numerical model PSEM_2D is applied to reproduce the experiments of *Elliot et al.* [1989]. Five different textured soils are selected. The experiments, including simulated rainfall and added flow in rills, correspond to period 2 in the WEPP database. Four sediment transport

capacity formulae are selected in the literature. These formulae do not require any calibration. The parameters of the first-order detachment transport coupling model come from the WEPP database. The hydrological and hydraulic parameters of PSEM_2D are calibrated manually so that the simulated water discharges and the average flow velocities are similar to the measured data. Under these conditions, the simulated sediment loads are compared with the observed sediment loads to evaluate the performance of the four sediment transport capacity formulae. Then the longitudinal erosion patterns are examined to explore the implication of the detachment-transport coupling model when it is associated to a 2D overland flow model that accounts for morphological changes.

2.1. Description of the Model

2.1.1. General Presentation

[7] PSEM_2D is a two-dimensional numerical model based on an explicit finite difference scheme coupling infiltration, overland flow and soil erosion processes. PSEM_2D is described in detail by *Nord and Esteves* [2005]. Below a short description is given. The development of PSEM_2D is an attempt to improve the understanding of the interactions between flow hydraulics and erosion processes at the plot scale. The erosion processes involved are rainfall and runoff detachment of original soil, rainfall redetachment, and overland flow entrainment of sediment from the covering cohesionless layer, and deposition. The formation of the covering cohesionless layer is related to rainfall impact before runoff and deposition of sediment by overland flow. Infiltration is computed using a Green and Ampt model. Overland flow is computed using the depth-averaged two-dimensional unsteady flow equations (Saint Venant equations). Sediment concentration is computed by combining the equation of mass conservation of sediment and the first-order detachment-transport coupling model. Coupling of runoff processes and erosion processes is made by computing the bed elevation at the end of each time step as a result of incision or deposition. Sediment concentrations are assumed to be small enough so as not to appreciably influence the mechanisms of flow [*Bennett, 1974*]. The friction slopes are estimated using the Darcy-Weisbach equations. The model uses a single representative particle size. The limits of using a single particle size class in this model is recognized. *Nord and Esteves* [2005] stated that it was a first step before further development of the model. Nevertheless, at this stage, the use of a single representative particle size allows to test in a simple way the validity of the equations applied. The implementation of a multiclass approach would require assumptions concerning the formulation of the sediment transport capacity as a function of particle size that are not yet tested.

2.1.2. Transport Capacity Formulae

[8] Four transport capacity formulae were selected in the literature as they have been shown to give acceptable results: the formula of *Yalin* [1963] based on shear stress, the formula of *Low* [1989] based on stream power, and two empirical formulae proposed by *Govers* [1992] based on unit stream power and effective stream power.

2.1.2.1. Formula of Yalin

[9] The *Yalin* [1963] equation is a classic excess shear stress bed load formula based on physical principles and

calibrated using experimental data collected in channels or rivers. It is defined as

$$T_c = A \left(\frac{\rho_s}{\rho} - 1 \right) \rho^{1/2} \tau^{1/2} D_s \quad (1)$$

in which T_c is the sediment transport capacity, ρ_s is the sediment density, ρ is the water density, τ is the total flow shear stress, D_s is the diameter of the sediment, g is the gravitational acceleration and

$$A = 0.635\gamma \left[1 - \frac{1}{\beta} \log(1 + \beta) \right] \quad (2)$$

$$\gamma = \frac{Y}{Y_{cr}} - 1 \quad (3)$$

$$\beta = \frac{2.45}{\left(\frac{\rho_s}{\rho} \right)^{0.4}} Y_{cr}^{0.5} \gamma \quad (4)$$

in which Y is the Shields number defined by

$$Y = \frac{\tau}{D_s(\rho_s - \rho)g} \quad (5)$$

and Y_{cr} is the critical value of the Shields number for incipient motion of sediment particles. In this study the values of Y_{cr} are determined using the Shields curve proposed by *Yalin and Karahan* [1979].

[10] The Yalin equation was incorporated in the erosion component of WEPP [*Foster et al.*, 1995] although relatively few attempts had been made to evaluate its performance in overland flow conditions [*Alonso et al.*, 1981; *Govers*, 1992; *Ferro*, 1998]. The Yalin equation was rearranged in a mathematical form useful to deduce an explicit relationship which estimates the transport coefficient of the transport equation of the WEPP model [*Foster et al.*, 1995]:

$$T_c = K_t \tau^{3/2} \quad (6)$$

in which K_t is the transport coefficient defined by

$$K_t = \frac{A}{Y \rho^{1/2} g} \quad (7)$$

2.1.2.2. Formula of Low

[11] The *Low* [1989] equation is a modified version of the formula of *Smart* [1984] that takes into account density effects. It can be expressed as follows:

$$T_c = \frac{6.42}{\left(\frac{\rho_s}{\rho} - 1 \right)^{0.5}} (Y - Y_{cr}) D_s S_f^{0.6} \bar{V} \rho_s \quad (8)$$

where S_f is the friction slope and \bar{V} is the depth-averaged flow velocity in the flow direction.

[12] According to *Govers* [1992] this formula is interesting since it is the only formula that has been developed using experimental data obtained on steep slopes, although

unit discharges were considerably higher and sediment sizes considerably coarser than those used in overland flow experiments. The method proposed by *Ferro* [1998] was used to transform *Low*'s formula as a stream power equation in which a stream power coefficient, depending on Shields parameter, slope, sediment and water density and flow depth, appears:

$$T_c = K_{SP} SP \quad (9)$$

in which SP is the stream power and K_{SP} is the stream power coefficient expressed as

$$K_{SP} = \frac{6.42 \frac{\rho_s}{\rho}}{\left(\frac{\rho_s}{\rho} - 1 \right)^{0.5}} \frac{(Y - Y_{cr})}{S_f^{0.4} g \frac{h}{D_s}} \quad (10)$$

where h is the flow depth.

[13] The ground slope S is systematically substituted by the energy slope S_f in this study.

2.1.2.3. Formula of Govers USP

[14] *Govers* [1992] also calibrated a unit stream power formula for particles of quartz of size between 58 and 218 μm :

$$T_c = \frac{86.7(S_f \bar{V} - 0.005)}{\sqrt{D_s}} q \quad (11)$$

where q is the unit flow discharge.

2.1.2.4. Formula of Govers ESP

[15] *Govers* [1992] calibrated an excess effective stream power formula on the basis of his data for particles of quartz of size between 127 and 414 μm . The equation is defined by

$$\log T_c = 1.081 \log \left(\frac{(\tau \bar{V})^{1.5}}{h^{2/3}} - \frac{(\tau_c \bar{V})^{1.5}}{h^{2/3}} \right) - 2.528 \quad (12)$$

in which $\frac{(\tau \bar{V})^{1.5}}{h^{2/3}}$ is the effective stream power and τ_c is the critical shear stress of the noncohesive particles.

[16] *Ferro* [1998] highlighted that the advantage of the effective stream power compared to the stream power is that it is function of the flow depth.

2.1.3. First-Order Detachment-Transport Coupling Model

[17] The model of soil detachment and deposition by runoff applied in PSEM_2D is the first-order detachment transport coupling model proposed by *Foster et al.* [1995]:

$$D_{fd,d} = K_r (\tau - \tau_{sol}) \left(1 - \frac{q_s}{T_c} \right) (1 - \epsilon) \quad (13)$$

$$D_{fd,e} = K_r (\tau - \tau_c) \left(1 - \frac{q_s}{T_c} \right) \epsilon \quad (14)$$

where $D_{fd,d}$ is the detachment/deposition rate of sediment from original soil by runoff, $D_{fd,e}$ the entrainment/deposition rate of sediment from the covering layer by runoff, K_r the flow erodibility parameter, τ_{sol} the critical shear stress of the cohesive soil, q_s the sediment discharge

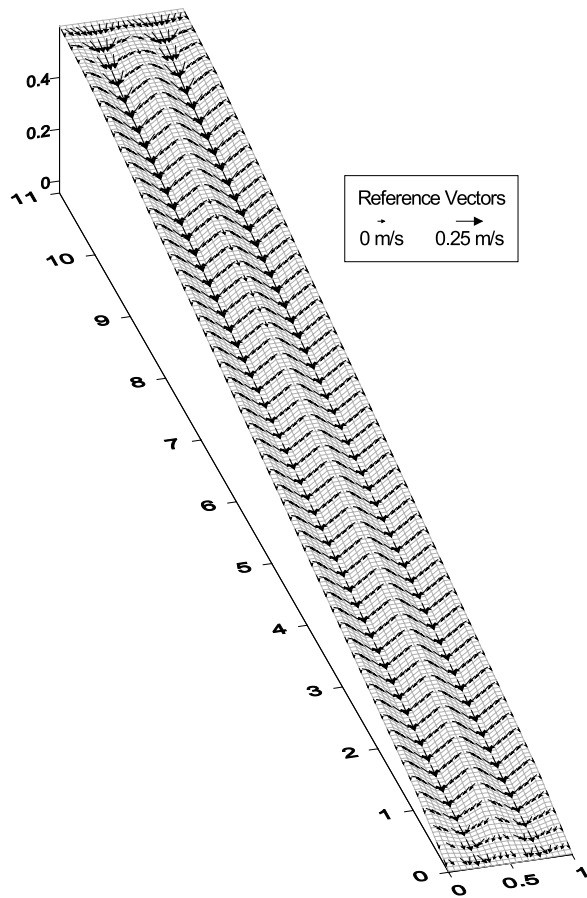


Figure 1. Velocity vectors for the Barnes_ND ($D_s = 115 \mu\text{m}$ and $\rho_s = 2000 \text{ kg m}^{-3}$) when the formula of Govers USP is used at 5 min after the beginning of period 2.

per unit flow width, and ϵ the percentage of a grid cell covered by the covering layer.

[18] K_r and τ_{soil} are the two most important parameters for this study. The total shear stress is assumed to contribute to both detachment and transport of sediment in this study. Other expressions than equations (13) and (14) are used to calculate the deposition rates [Nord and Esteves, 2005].

2.1.4. Boundary Conditions at the Upper End of the Rills

[19] The boundary conditions are crucial in this study. The conditions at the downstream end were given by Nord and Esteves [2005]. At the upper end, a flow discharge is

injected. At this limit we control the flow discharge delivered and we compute the water depth using the kinematic wave approximation. The longitudinal velocity is derived from the flow discharge and the flow depth. The transversal velocity is assumed to be zero. There is no sediment concentration injected at the upper end.

2.2. Numerical Experiments

2.2.1. Standard Topography

[20] The standard topography used in this study is similar to that described by Elliot *et al.* [1989]. The initial shape of the rills is 9 m long, 0.5 m wide and 0.05 m deep with a uniform trapezoidal cross section. Their standard profile presents a 0.1 m wide trough and two adjacent ridges of 0.05 m wide connected to the trough by side slopes as shown in Figure 1. The spatial resolution is 0.05 m in the two horizontal directions. The five soils selected from the WEPP database are the Amarillo, the Pierre, the Barnes_ND, the Bonifay and the Collamer soils. For each soil, Elliot *et al.* [1989] worked with three pairs of rills formed using a ridging tool mounted on a small tractor. In this study a pair of identical rills is considered for each soil as shown in Figure 1 and the longitudinal slope is calculated as the average of six rills. The longitudinal slopes range from 3 to 9% as shown in Table 1. The rills are extended 1 m upstream the upper end and 1 m downstream the lower end to improve the treatment of the boundary conditions as shown in Figure 1. The whole length of the rills is therefore 11 m. The flow discharge is injected over the whole width of the upper limit. The flow naturally converges toward the troughs of the depressions as indicated by the velocity vectors in Figure 1. This zone of convergence allows avoiding the local injection of the flow discharge straight into the troughs of the rills. As clear water is injected and flow discharge may be as high as 40 L min^{-1} in a single rill, erosion would be accentuated at the upper reach of the rill if flow was injected over the three lowest nodes of the rill profile. This would cause numerical instabilities or numerical shocks as a result of rapidly changing surface slopes. A similar divergence zone is included at the end of the rills to prevent from regressive erosion. Govers [1992] observed that the drawdown of the water surface near the flume outlet was such that sediment transport was intensified, so that excessively high sediment transport rates were measured.

[21] The geometrical characteristics of the rills applied in this study are common in the literature. In the experimental study carried out by Polyakov and Nearing [2003], the rill was 8 m long and 0.61 m wide and a slight V shape with

Table 1. Input Parameters Including the Water Temperature, the Average Slope, the Sediment Properties D_{50} and ρ_s , and the Parameters of the Detachment-Transport Coupling Model τ_{soil} and K_r ^a

Soil Name	Water Temperature, deg C	Average Slope, %	D_{50} Texture, μm	D_{50} Undispersed Eroded Sediment, μm	ρ_s Undispersed Eroded Sediment, kg m^{-3}	τ_{soil} , Pa	K_r , s m^{-1}
Amarillo	23.5	3.59	230	150	2650	1.6	0.0356
Pierre	27.0	6.65	4	280	2000	4.8	0.0109
Barnes_ND	22.5	5.78	28	115	2000	2.5	0.0032
Bonifay	26.0	3.98	310	200	2650	1.0	0.0157
Collamer	19.0	8.68	14	45	2000	6.3	0.0215

^aThe values of τ_{soil} and K_r come from the WEPP database [Elliot *et al.*, 1989].

Table 2. Calibration of the Infiltration Parameters K_s and h_f and the Friction Factor f in Rill Eroding Conditions Using the Low Equation^a

Soil Name	K_s , m s ⁻¹	h_f , m	f Calibrated for Each Added Flow Rate					
			7 L min ⁻¹	14 L min ⁻¹	21 L min ⁻¹	28 L min ⁻¹	35 L min ⁻¹	42 L min ⁻¹
Amarillo	$2.0E^{-6}$	0.22	0.6	0.6	NR	NR	NR	x
Pierre	$1.5E^{-7}$	2.00	0.8	1.0	1.1	1.1	1.2	x
Barnes_ND	$3.0E^{-6}$	0.20	0.9	0.95	1.0	1.0	0.95	0.9
Bonifay	$2.0E^{-5}$	0.12	0.8	0.7	0.6	NR	NR	x
Collamer	$1.2E^{-7}$	1.10	1.0	1.2	1.6	2.1	2.3	x

^aHere f is calibrated for each soil and for each flow rate, NR means that the simulation stopped before reaching this step, and x means not tested by *Elliot et al.* [1989].

approximately 2% side slopes was formed initially. In another study undertaken by *Gimenez et al.* [2004], the rill was 4.5 m long, 0.4 m wide and was shaped by a 0.05 m deep longitudinal central depression with a flat bottom. It is therefore possible to refer to these studies for comparing the results in terms of unit water discharges, sediment concentration or morphological evolution of rills.

2.2.2. Calibration of Infiltration and Flow Hydraulics

2.2.2.1. Infiltration

[22] Infiltration is computed using a Green and Ampt equation described in details by *Esteves et al.* [2000]. The infiltration parameters are the hydraulic conductivity at natural saturation K_s , the wetting front capillary pressure head h_f , and the initial and saturated volumetric water contents θ_s and θ_i respectively. The use of a Green and Ampt equation is questionable, especially in the case of the clay soils. However, our purpose is only to reproduce the flow rates measured during period 2 of the experiments of *Elliot et al.* [1989] without attempting to reproduce the transient regime of infiltration observed during the beginning of period 1 before runoff equilibrium. The soils are assumed to be saturated during period 2 and the infiltration rates are nearly constant. We calibrate the values of the hydraulic conductivity and the wetting front capillary pressure head using the average discharge of six rills for each soil. The adjusted parameters are given in Table 2. The simulated water discharges are compared with the observed values at the end of the real rills, i.e., before entering the divergence zone, 1 m upstream of the lowest end in Figure 1.

2.2.2.2. Flow Hydraulics

[23] A look at the values of the Darcy-Weisbach friction factors f derived by *Elliot et al.* [1989] shows that the $f-Re$ relationships are complex. Therefore Re is not a sufficient predictor of hydraulic roughness in eroding rills. Predictive relationships for estimating the friction factor cannot be used unless abundant soil information is obtained [*Nearing et al.*, 1997]. A global friction factor calibrated in rill eroding conditions using the Low equation was considered to be more preferable for this work. We used a spatially uniform friction factor over the whole grid of the paired rills. The simulated velocities of the points located in the middle of the cross section, i.e., at the bottom of the V shape, were averaged over the last 6 m of the 9 m rills and compared to the average flow velocities of six rills for each soil. As it was not possible to reproduce the observed flow velocities using a unique value of the friction factor, we calibrated it for each inflow rate and for each soil. Therefore flow hydraulics was allowed to change during a simulation

run as a function of flow discharge and related incision/deposition. An increase of the calibrated friction factor with the added inflow rate may be interpreted as energy expenditure because of additional losses such as hydraulic jumps. In reverse, a decrease of the calibrated friction factor when the added flow rate increases may mean that the rill is smoothing or widening due to bank sloughing for example. Such processes are not described explicitly in the model but are lumped within the global friction factor. The computation of the flow width depends on the flow rate, the slope, the friction factor and the shape of the cross section of the rill. Generally only the lower point of the cross section located at the bottom of the V shape, has flow shear stresses high enough to overcome the critical shear stress of the cohesive soil and produce incision/deposition. As a consequence, our model was more prone to erosion by deepening than erosion by widening. Effects of sediment load on flow hydraulics were not included as the experimental evidence is inconclusive [*Govers*, 1992; *Guy et al.*, 1992; *Merten et al.*, 2001].

[24] The values of the calibrated friction factor are given in Table 2. The added flow rates ranged from 7 to 35 L min⁻¹ for all the soils except the Barnes_ND which ranged from 7 to 42 L min⁻¹. Low values of the friction factor are associated to the Bonifay and the Amarillo soils which are noncohesive soils. f is about 0.6 for the Amarillo soil and between 0.6 and 0.8 for the Bonifay soil with a decreasing trend when the flow discharge increases. These values are lightly higher than those derived by *Elliot et al.* [1989] using their measured data. The Pierre, the Barnes_ND, and the Collamer soils which are cohesive soils demonstrate larger friction factor values, characterized by high roughness. For the Pierre soil, f is between 0.8 and 1.2 and increases along with the flow discharge. For the Barnes_ND soil, f is relatively stable and is between 0.9 and 1.0. The Collamer soil is the roughest soil with f increasing from 1.0 for the lowest inflow rate to 2.3 for the highest inflow rate.

[25] The values of the measured velocities and the velocities computed using the Low equations are given in Table 3. The results show the capacity of the calibration procedure to reproduce the measured velocities over a wide range of flow conditions.

2.2.3. Sediment Properties and Parameters of the Detachment-Transport Coupling Model

[26] The rill erodibility parameter K_r and the critical shear stress for cohesive soil τ_{soil} come from the WEPP database, presented in Table 1. These parameters were calibrated by *Elliot et al.* [1989] by linear regression using the equations

Table 3. Measured and Simulated Velocities^a

	Added Flow Rates					
	7 L min ⁻¹	14 L min ⁻¹	21 L min ⁻¹	28 L min ⁻¹	35 L min ⁻¹	42 L min ⁻¹
Amarillo	0.245 0.234	0.277 0.272	0.545 NR	0.637 NR	0.708 NR	x
Pierre	0.277 0.275	0.294 0.294	0.303 0.304	0.330 0.325	0.333 0.338	x
Barnes_ND	0.240 0.240	0.268 0.275	0.278 0.285	0.297 0.300	0.312 0.319	0.335 0.341
Bonifay	0.191 0.196	0.252 0.254	0.318 NR	0.362 NR	0.378 NR	x
Collamer	0.287 0.285	0.320 0.313	0.308 0.314	0.298 0.306	0.303 0.311	x

^aThe velocities are expressed in m s⁻¹. The measured velocities correspond to the average flow velocity of six rills. The simulated velocities are averaged over the last 6 m of the 9 m rills. They were obtained using the Low equation. NR means that the simulation stopped before reaching this step, and x means not tested by *Elliot et al.* [1989].

of the rill erosion component and observed data. The rainfall detachment and rainfall redetachment were not considered in this study as we assume that its effect on sediment transport was negligible during period 2 of the experiment of *Elliot et al.* [1989]. *Ferro* [1998] assessed the influence of rainfall on sediment transport capacity on the basis of various studies of the literature and recalled that the rainfall contribution to total transport becomes negligible when the flow depth is greater than three times the raindrop diameter [*Sharma et al.*, 1993]. The other parameters necessary in PSEM_2D are the median particle diameter of the sediment D_{50} , the water temperature, the sediment density ρ_s , the water density ρ , and Φ a coefficient that accounts for the degree of mixing of the sediment concentration within the flow depth. The D_{50} of the soil matrix and of the undispersed eroded sediment along with the water temperature are given in Table 1. These values result from an analysis carried out by the authors on the comparison between the particle size distributions of the soil matrix and the undispersed eroded sediment. During the calibration phase, the D_{50} of the soil matrix and a sediment density of 2650 kg m⁻³ were used. Subsequently, the same simulations were run with the D_{50} and the density of the undispersed eroded sediment. ρ_s was 2650 kg m⁻³ in the case of the Amarillo and Bonifay soils since these soils were mostly eroded as primary particles. The Pierre, Barnes_ND, and Collamer soils were mostly eroded as aggregates. Therefore ρ_s was set to 2000 kg m⁻³ according to the values measured by [*Davis et al.*, 1983; *Rhoton et al.*, 1983; *Foster et al.*, 1985] for the density of aggregates. The water density is a function of the temperature. Turbulence is high enough to mix the sediment concentration within the flow depth. The value of Φ is therefore set to 1.

3. Results and Discussion

3.1. Hydraulics

[27] The friction factors calibrated using the Low formula and presented in Table 2 were then applied using the three other transport equations described in section 2.1.2. The observed and the calculated velocities are plotted in Figure 2. The results show that, for each soil, the calculated velocities corresponding to the four transport capacity formulae are not distinguishable at the beginning of the simulation. They differentiate as the inflow rate increases resulting from the changes in bed morphology due to incision or deposition. The changes in bed morphology

are controlled by the detachment-transport coupling model dependent on the transport equation applied. The unexpected falls of the simulated velocities over a short period of time after injections of larger inflow rates for the Pierre, the Barnes_ND, and the Collamer soils are due to numerical oscillations when the upstream boundary condition and the friction factor changed. The model is more sensitive to instabilities when f is larger than 1.0.

[28] The calculation and the calibration of flow hydraulics are key points in this study. Although the calibration procedure provides acceptable results, it is very much simplified compared with the complexity of the real processes. Average flow conditions are simulated by the St Venant equations because of the use of a spatially uniform friction factor for each soil and for each flow rate. Various energy losses are implicitly parameterized within the global friction factor. *Gimenez et al.* [2004] clearly showed that flow hydraulics is spatially nonuniform. The authors observed that the bed of an eroding rill formed a succession of steps and pools with rapid transitions from supercritical to subcritical flow due to the changes in topography. *Nearing et al.* [1997] asserted that given the importance of local turbulence and localized supercritical flows associated with the rilling process, the interpretation of average flow information is questionable. Nevertheless, *Gimenez and Govers* [2002] showed that average flow conditions are good predictors of flow detachment. Simulation of nonaverage flow conditions using the Navier-Stokes equations is far beyond the scope of this paper and available observed data are inadequate to such an exercise.

3.2. Sediment Transport Capacity

[29] Figure 3 presents the simulated sediment delivery (Q_s) as a function of time for the five soils selected in this study when the four transport equations described in section 2.1.2 are applied. The results are given for two median sediment diameters. On the left-hand side, the simulations were run with the D_{50} of the soil matrix and a sediment density of 2650 kg m⁻³. On the right-hand side, the simulations were run with the D_{50} and the density of the undispersed eroded sediment. Incomplete simulations due to numerical problems are to be dealt with later on. Figure 3 reveals that globally the calculated sediment loads are quite similar and of the same order of magnitude as the observed data considering the scattering of the observed data.

[30] The irregularities of the calculated sediment deliveries near the end of the simulations for the Pierre, the Barnes_ND, and the Collamer soils are due to numerical

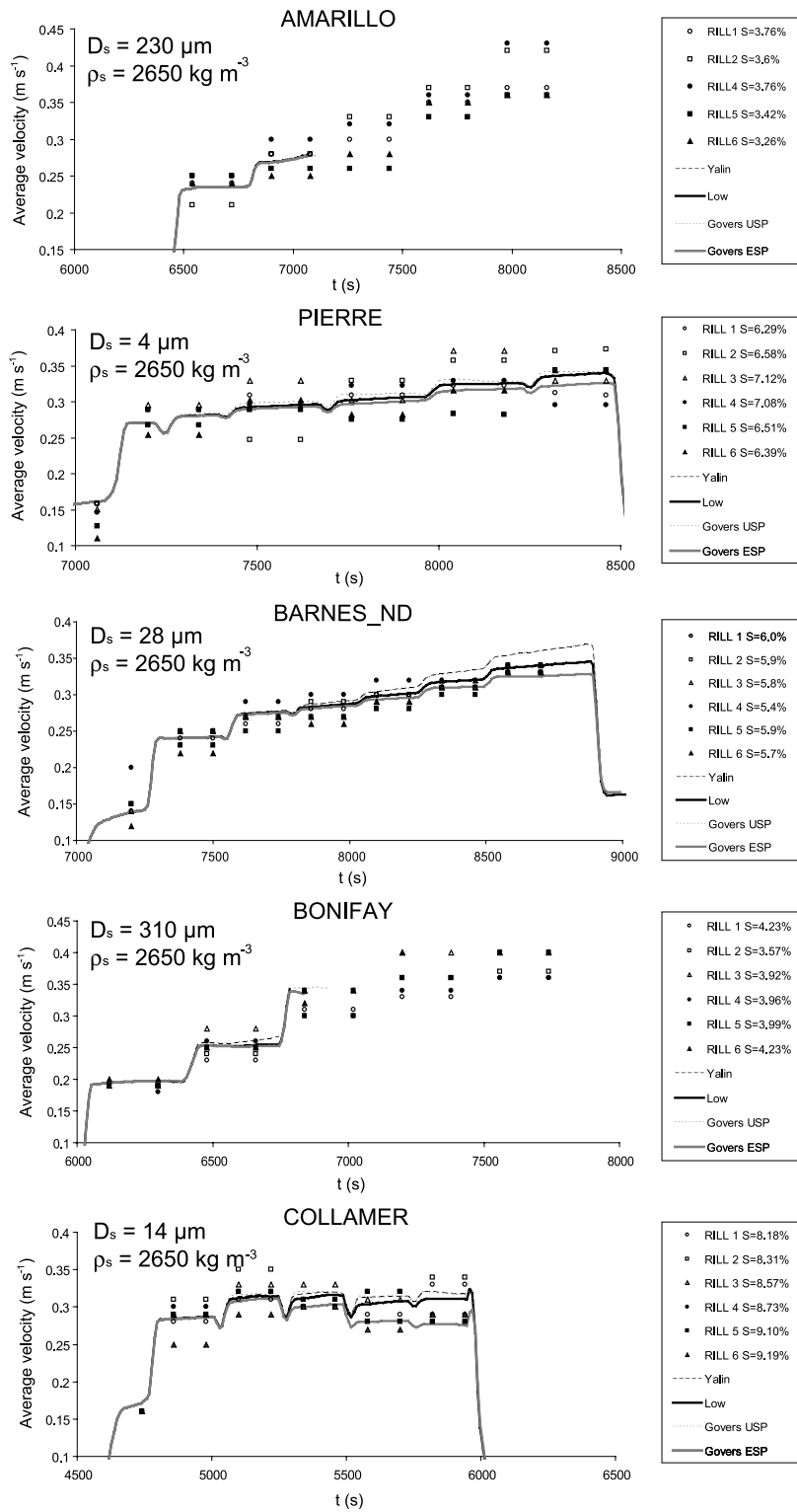


Figure 2. Observed and calculated velocities for the five soils during period 2 of the experiment of *Elliot et al.* [1989].

problems. In the convergence zones where erosion rates are important and topography is changing rapidly, the model is occasionally unsuccessful in redistributing the sediment mass. In some cases, side slopes were very steep. This caused sediment concentration to become superior to 1.0 over short periods of time and lead to instabilities of

the sediment delivery. Therefore the sediment load corresponding to these periods should not be taken into account in the analysis.

[31] A necessary condition to evaluate the sediment transport formulae is the presence of a transport-limiting regime. This is the case for all soils except the Barnes_ND

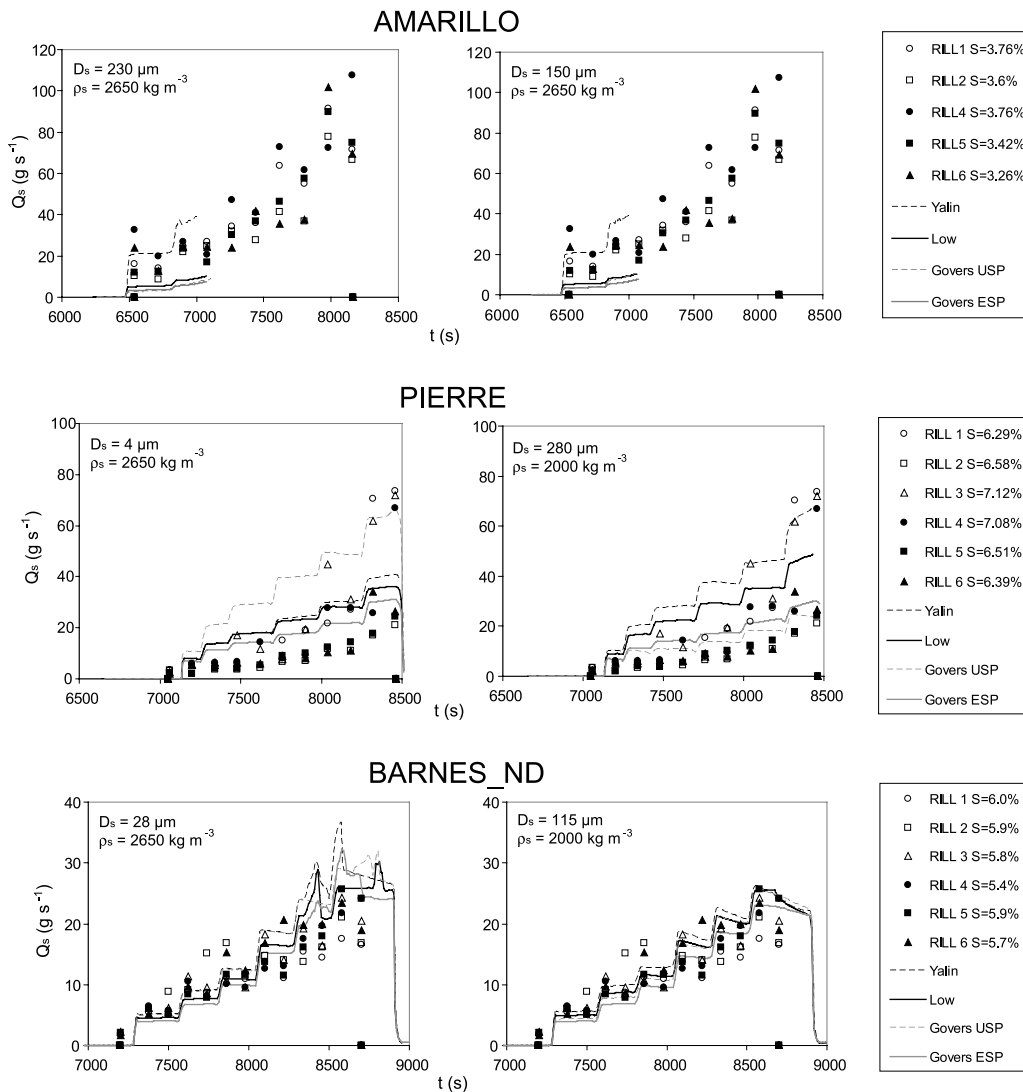


Figure 3. Observed and calculated sediment loads for the five soils during period 2 of the experiment of *Elliot et al.* [1989]. The curves displayed in the graphs on the left-hand side are obtained using the D_{50} of the soil matrix, and the curves displayed in the graphs on the right-hand side are obtained using the D_{50} of the undispersed eroded sediment.

soil. For this latter soil, the sediment loads calculated using the four transport equations are quite similar and the regime is rather limited by detachment. This is not surprising considering the parameters of the detachment/deposition model applied to this soil in Table 1. The rill erodibility parameter K_r has the lowest value of the group. The results corresponding to this soil are therefore not considered for the transport equations evaluation.

[32] For the Amarillo and the Bonifay soils, which are noncohesive soils mostly eroded as primary particles, the results behave similarly. There is no difference between the results of the graphs on the left- and right-hand sides of Figure 3 since the size and the density of the particles of the soil matrix are nearly the same as those of the undispersed eroded sediment (see Table 1). The Yalin formula slightly overestimates the observed sediment loads whereas the three other formulae give comparable results and underestimate the results.

[33] For the Pierre soil, which is a cohesive soil mostly eroded as aggregates, 2 orders of magnitude were observed between the D_{50} of the soil matrix and the D_{50} of the undispersed eroded sediment. When the D_{50} of the soil matrix is applied ($D_{50} = 4 \mu\text{m}$) with a particle density of 2650 kg m^{-3} , the four transport equations give higher sediment loads compared to the observed values as seen in the graph on the left-hand side of Figure 3. The Govers USP formula overestimates significantly the results whereas the Yalin, the Low and the Govers ESP formulae slightly overestimate the results. When the D_{50} of the undispersed eroded sediment is applied ($D_{50} = 280 \mu\text{m}$) with a particle density of 2000 kg m^{-3} (graph on the right-hand side of Figure 3), the Govers USP gives relatively good results, while the Govers ESP formula still overestimates lightly the results, the Low formula provides higher sediment loads and the Yalin formula overestimates largely the results.

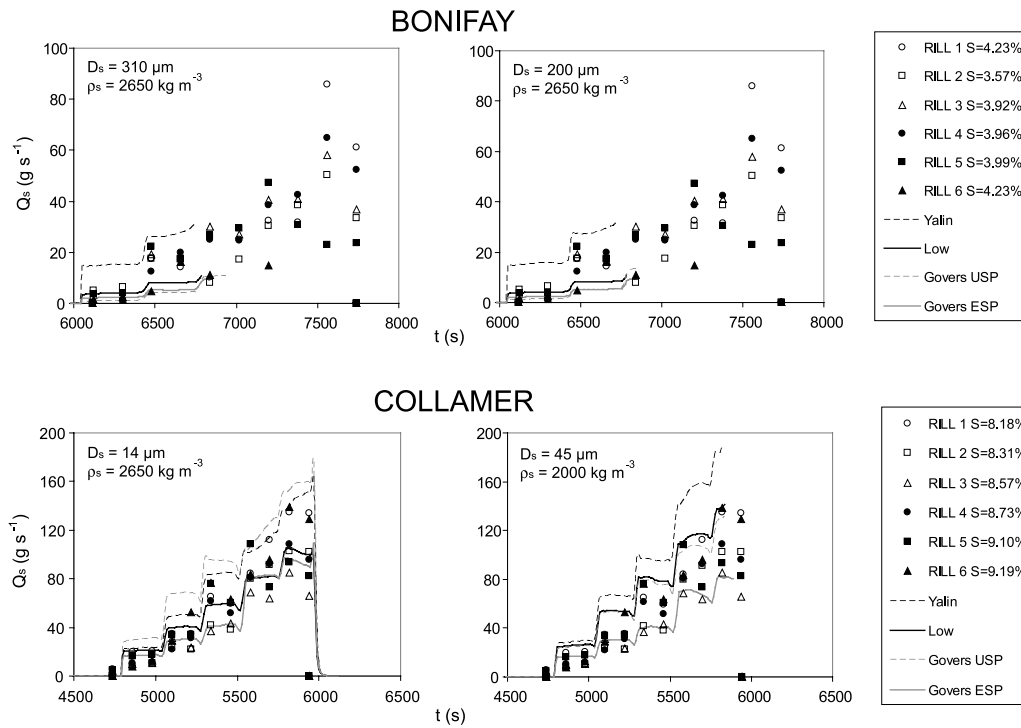


Figure 3. (continued)

[34] For the Collamer soil, which is a cohesive soil eroded as both primary particles and aggregates, the results behave quite in the same way as for the Pierre soil. The D_{50} of the undispersed eroded sediment is three times larger than the D_{50} of the soil matrix. When the D_{50} of the soil matrix is applied ($D_{50} = 14 \mu\text{m}$) with a particle density of 2650 kg m^{-3} , the Yalin and the Govers USP formulae overestimate the observed sediment loads whereas the Govers ESP and the Low formulae give relatively good results. When the D_{50} of the undispersed eroded sediment is applied ($D_{50} = 45 \mu\text{m}$) with a particle density of 2000 kg m^{-3} , the Govers USP formula gives acceptable results, the Low formula overestimates somewhat the observed data,

the Yalin formula overestimates considerably the results and the Govers ESP underestimates slightly the results.

[35] Different values of the particle size and density of sediment were applied in this study to counteract the limitation related to the use of a single representative median sediment size. Looking at the results of Figure 3 and the mathematical expressions of the sediment transport capacity formulae presented above, one can address the sensitivity of these formulae to the variations of the sediment diameter and the sediment density. The Yalin equation is not as sensitive to the sediment density as it is to the sediment diameter. The relationship between the sediment diameter and the sediment transport capacity is complex and not intuitive. The sediment transport capacity increases with

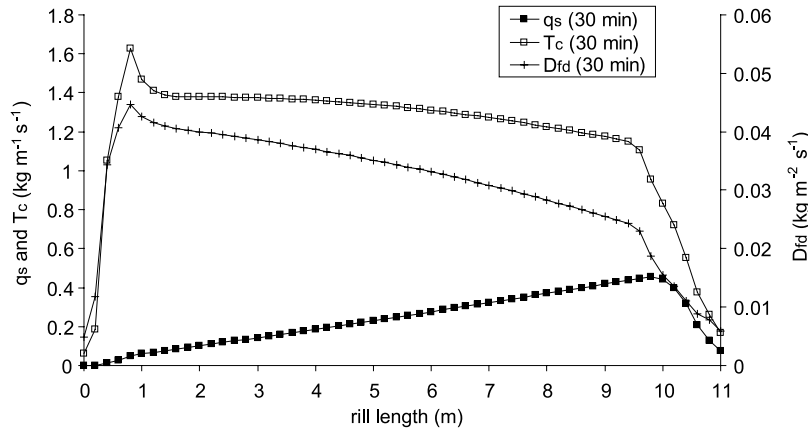


Figure 4. Calculated sediment load (q_s), sediment transport capacity (T_c), and detachment or deposition rate (D_{fd}) along the rill length for the Barnes_ND ($D_s = 115 \mu\text{m}$ and $\rho_s = 2000 \text{ kg m}^{-3}$) when the formula of Govers USP is used at 30 min after the beginning of the simulation.

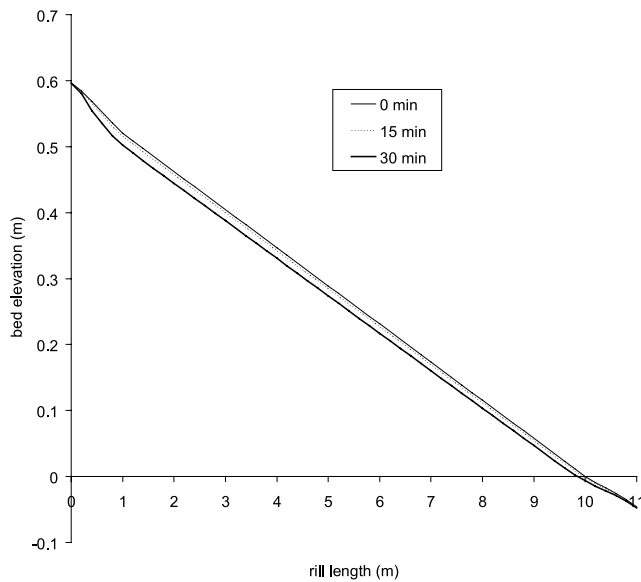


Figure 5. Evolution of calculated soil surface elevation with time along the rill length for the Barnes_ND ($D_s = 115 \mu\text{m}$ and $\rho_s = 2000 \text{ kg m}^{-3}$) when the formula of Govers USP is used.

increasing sediment diameter for fine particles (inferior to $50 \mu\text{m}$) and then decreases slowly with increasing sediment diameter for coarser particles. For the Low equation, the sediment transport capacity increases with decreasing sediment density. However, it is not sensitive to the sediment diameter. The Govers USP equation gives much lower values for increasing sediment diameter as it is proportional to the inverse of the square root of the diameter. However, this equation is not a function of the sediment density as it was developed empirically using only quartz particles [Govers, 1992]. The Govers ESP depends on both the sediment diameter and the sediment density through the use of τ_c in equation (12). However, this equation is neither sensitive to the sediment density nor to the sediment diameter.

[36] All these formulae were originally developed for bed load conditions except the Govers USP which can explain its strong sensitivity to the sediment size. The Yalin and the Low formulae were derived from physical principles and

calibrated using empirical data. The Govers USP and Govers ESP formulae were calibrated by using only empirical data. The Yalin and the Low formulae were initially proposed by researchers involved in sediment transport by rivers whereas the Govers USP and the Govers ESP formulae were developed specifically for sediment transport by overland flow.

[37] The results show that the Govers USP formula, which has a simple expression, performs the best in eroding conditions over cohesive soils. This equation is very sensitive to the sediment diameter, which is a necessary condition to assure that the characteristics of aggregates are taken into account in the sediment transport models. The Yalin equation should not be used in rill flow conditions. The calibration of the transport coefficient K_t defined in equation (7) is not appropriate to overland flow conditions. Furthermore this equation is very sensitive to the computation of the shear stress. In this study, the total shear stress is used to compute both the detachment term and the sediment transport capacity. A possible alternative might be to use grain shear stress. However, identifying grain shear stress is difficult [Govers, 1992] and while grain shear stress may be a valid parameter for sediment transporting capacity [Govers and Rauws, 1986], it is not the case for soil detachment [Gimenez and Govers, 2002]. The Low and the Govers ESP formulae can be used to provide a good estimation of the total sediment load by concentrated flow in rills. However, they cannot provide information on the size selectivity of sediment transport as they are not sensitive to the sediment diameter.

[38] In the case of the noncohesive soils, none of the equations tested performs well. Since the simulations are unstable and stop early, the simulations obviously miss physical processes. A possible explanation is that the physical principles involved in the first-order detachment-transport coupling model and its parameterization do not represent correctly the way these soils are eroded. What was observed on these soils by Elliot *et al.* [1989] is that sandy rills tend to erode by widening and silt and clay rills by deepening. The patterns of erosion along the rills produced by the model are discussed below. However, the validity of the detachment-transport coupling concept cannot be tested since no relevant data on the evolution of the topography of the rills are available in the WEPP database.

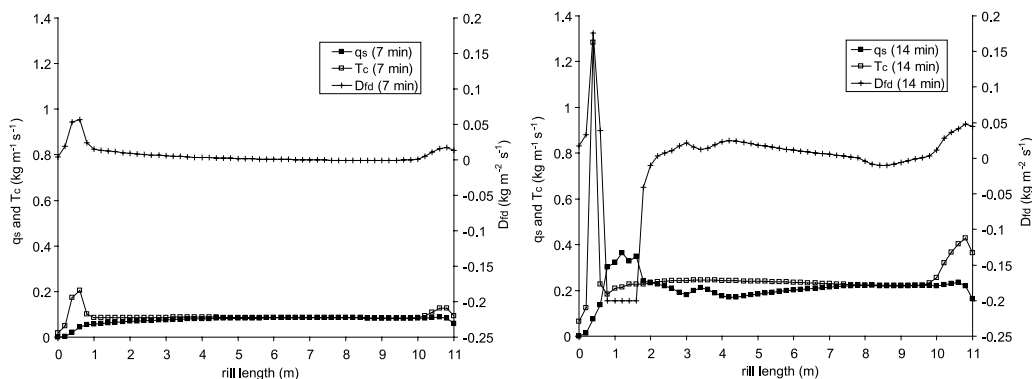


Figure 6. Calculated sediment load (q_s), sediment transport capacity (T_c), and detachment or deposition rate (D_{fd}) along the rill length for the Bonifay ($D_s = 200 \mu\text{m}$ and $\rho_s = 2650 \text{ kg m}^{-3}$) when the formula of Low is used, at 7 and 14 min after the beginning of the simulation.

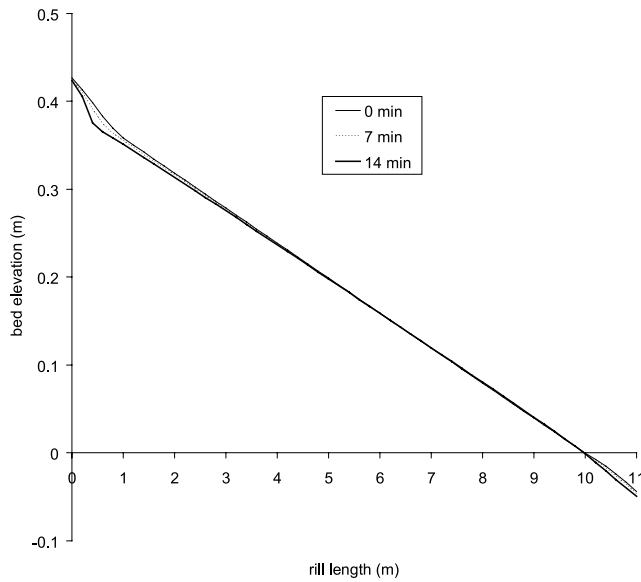


Figure 7. Evolution of calculated soil surface elevation with time along the rill length for the Bonifay ($D_s = 200 \mu\text{m}$ and $\rho_s = 2650 \text{ kg m}^{-3}$) when the formula of Low is used.

3.3. Detachment/Deposition Model

[39] This section presents a demonstration of how the coupling affects the spatial erosion patterns. Three cases representing three different situations are considered. The case of the Barnes_ND soil is first considered as this soil illustrates the detachment limiting regime. The analysis is limited to the results obtained with the Govers USP formula and the D_{50} of the undispersed eroded sediment. The case of the Bonifay soil is then examined. It is representative of the noncohesive soils in a transport limiting regime. The analysis involves the results obtained with the Low formula and the D_{50} of the eroded sediment. Finally the case of the Collamer soil is explored, looking at the results obtained with the Govers USP formula and the D_{50} of the undispersed eroded sediment.

[40] For the Barnes_ND soil, both the observed and calculated sediment loads are the lowest of the five soils as shown in Figure 3. Figure 4 shows the sediment load, the

transport capacity, and the detachment rate in the middle of the cross section, i.e., at the bottom of the V shape, along the rill for the highest inflow rate. The sediment load increases with the downslope distance but remains lower than the sediment transport capacity, illustrating a detachment limiting regime. The Froude number is inferior to 1.0 translating to a subcritical flow along the rill. Figure 5 shows the erosion profile resulting from the parameterization of the detachment-transport coupling model ($K_r = 0.0032 \text{ s m}^{-1}$, $\tau_{soil} = 2.5 \text{ Pa}$). The erosion cavity is spread over the whole length of the rill but remains relatively smooth. It is about 2 cm in 30 min in the most erosive zone located near the upper end.

[41] The Bonifay soil illustrates the case of the noncohesive soils in a transport limiting regime. Figure 6 gives the sediment load, the transport capacity, and the detachment rate in the middle of the cross section along the rill at two time steps during the simulation. The first graph corresponds to the end of the lowest inflow rate injection. The second graph corresponds to the period just before the early stop of the simulation. In the first graph the sediment load joins the transport capacity within the five first meters of the rill and remains constant downstream, leading to a detachment rate close to zero over the most part of the rill. In the second graph the transport capacity and the detachment rates display a strong peak followed by a significant fall in the first meter of the rill. As a consequence the sediment load becomes higher than the transport capacity and there is deposition over the second meter of the rill. In such a case, the detachment/deposition rate is arbitrary limited to $0.2 \text{ kg m}^{-2} \text{ s}^{-1}$ in the model in order to avoid excessive localized erosion or deposition. Downstream, the sediment load joins the transport capacity and the detachment rate tends to zero before a last increase at the divergence zone, responsible for erosion at the lower end. *Nearing et al.* [1997] observed that for noncohesive material, the rills had approximately reached a transport limiting state within a flow length of 3 m. The couple of parameters ($K_r = 0.0157 \text{ s m}^{-1}$, $\tau_{soil} = 1.0 \text{ Pa}$) applied to the Bonifay soil produces a localized erosion zone in the first meter of the rill. However, over the most part of the rill, the bed surface is constant as shown in Figure 7. A very high cavity volume in the first section was also observed by *Nearing*

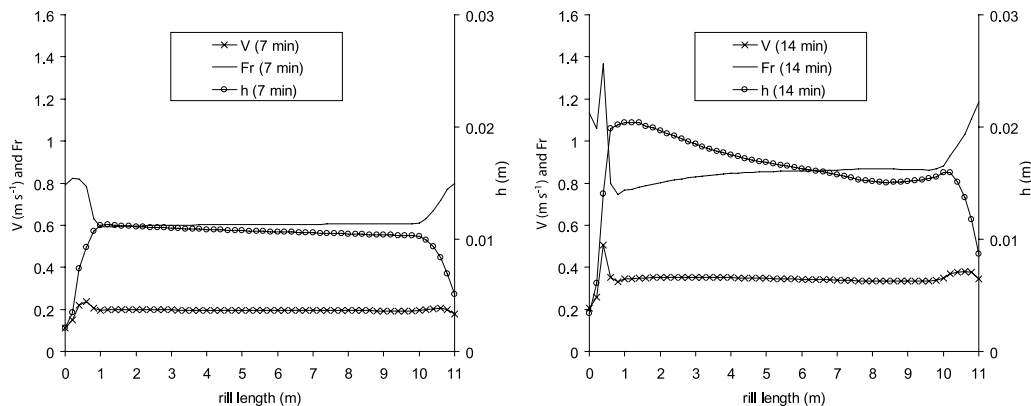


Figure 8. Calculated longitudinal velocity, Froude number, and water depth along the rill length for the Bonifay ($D_s = 200 \mu\text{m}$ and $\rho_s = 2650 \text{ kg m}^{-3}$) when the formula of Low is used, at 7 and 14 min after the beginning of the simulation.

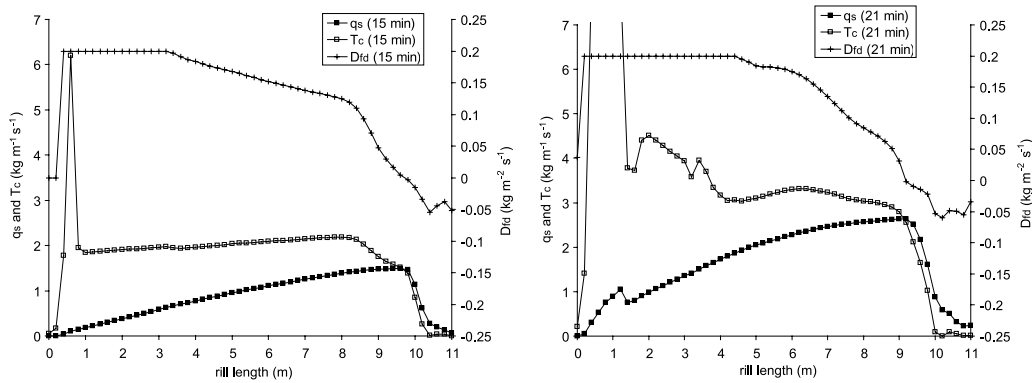


Figure 9. Calculated sediment load (q_s), sediment transport capacity (T_c), and detachment or deposition rate (D_{fd}) along the rill length for the Collamer ($D_s = 45 \mu\text{m}$ and $\rho_s = 2000 \text{ kg m}^{-3}$) when the formula of Govers USP is used, at 15 and 21 min after the beginning of the simulation.

et al. [1997]. The authors attributed this feature to boundary effects where the water first entered the soil bed. As shown in Figure 8, the Froude number was always less than 0.8 along the rill at the time 7 min, so the flow was only subcritical. At the time 14 min, the Froude number was less than 1.0 over most of the rill but reached values higher than 1.0 both at the upper and the lower ends of the rill. The flow was therefore supercritical upstream, then subcritical and supercritical again downstream. The resulting hydraulic jump affects the flow velocity and flow depth distributions along the rill and leads to a numerical shock and the early stop of the simulation.

[42] The Collamer soil is representative of the cohesive soils in a transport-limiting regime. Figure 9 shows the sediment load, the transport capacity, and the detachment rate in the middle of the cross section at two time steps of the simulation: during the injection of the third inflow rate and just before the early stop of the simulation. In the two graphs, the sediment loads increase along the rill but remain smaller than the transport capacities except at the lower end of the rill where deposition occurs. In the two graphs, the detachment rates reach the limit of $0.2 \text{ kg m}^{-2} \text{ s}^{-1}$ over 3 and 4 m downstream of the upper end of the rill then decrease downstream and become negative near the lower end of the rill. The two parameters ($K_r = 0.0215 \text{ s m}^{-1}$, $\tau_{soil} = 6.3 \text{ Pa}$) applied to the Collamer soil produce a deep and narrow cavity spread out along most of the rill and a deposition cone at the lower reaches of the rill as shown in Figure 10. The longitudinal eroded profile tends to a concave shape. More downslope distance is needed for the sediment load to join the transport capacity in this case compared with the Bonifay soil. This may partly be explained by the higher initial slope of the rill for the Collamer soil compared with the Bonifay soil (8.68% versus 3.98%) leading to large values of the sediment transport capacity as seen in Figure 9. Erosion is very intense upstream. The cavity reaches up to 8 cm deep, longitudinal slopes rise up to 26% before the early stop of the simulation and a hydraulic jump occurs between the time 15 min and the time 21 min as illustrated by Figure 11 followed by the unexpected stop of the simulation.

[43] The analysis of the results reveals that very different erosion patterns may be simulated by PSEM_2D. The

results presented in this study are consistent with the observations made by *Huang et al.* [1996] in a field experiment involving rills. *Huang et al.* [1996] described three situations very similar to the three sediment regimes discussed in this section. *Merten et al.* [2001] observed that in each experimental test, a portion of the rill bed experienced net detachment and a portion experienced net deposition. Looking at their numerical results, *Lei et al.* [1998] stated that the narrow areas of the rills were apparently scouring the surface, while the wider regions were experiencing sediment deposition, and the two types of regions alternated down the rill length.

[44] The early stops of the simulations mentioned above are related to the occurrence of hydraulic jumps that cannot be handled by the St Venant equations since these equations assume a gradually varying free surface. A three-dimensional

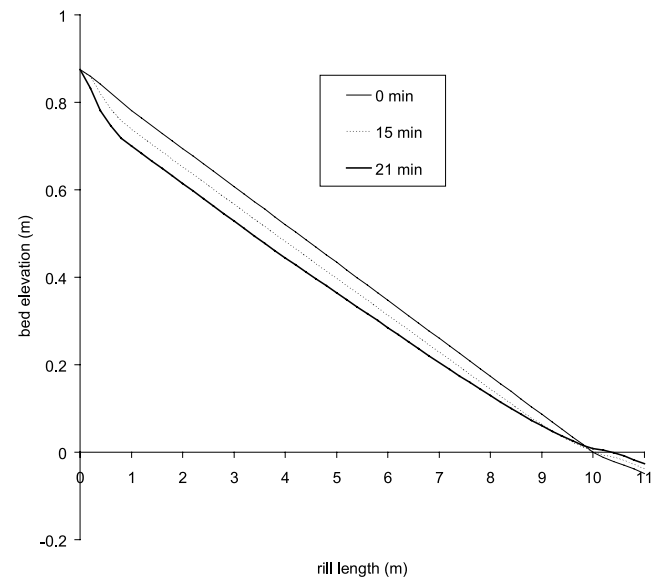


Figure 10. Evolution of calculated soil surface elevation with time along the rill length for the Collamer ($D_s = 45 \mu\text{m}$ and $\rho_s = 2000 \text{ kg m}^{-3}$) when the formula of Govers USP is used.

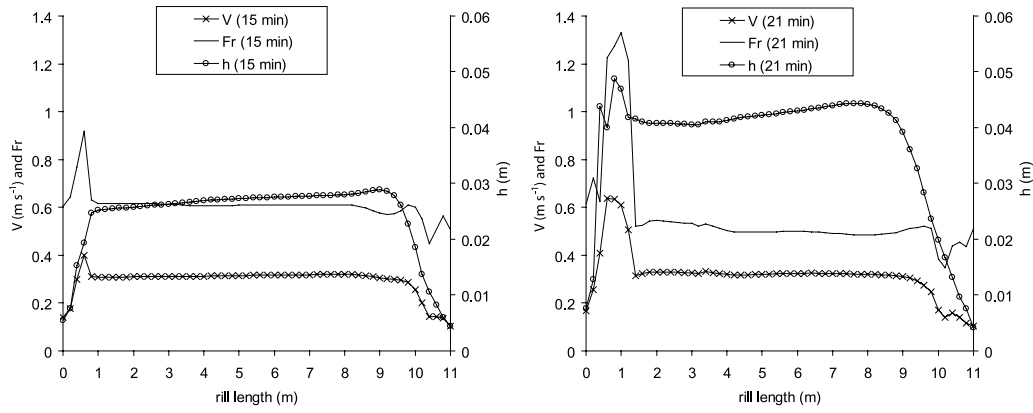


Figure 11. Calculated longitudinal velocity, Froude number, and water depth along the rill length for the Collamer ($D_s = 45 \mu\text{m}$ and $\rho_s = 2000 \text{ kg m}^{-3}$) when the formula of Govers USP is used, at 15 and 21 min after the beginning of the simulation.

model solving the complete Navier-Stokes equations would be required to avoid the numerical instabilities due to the hydraulic jumps but the available observed data would not support such an approach.

4. Conclusion

[45] PSEM_2D was used to simulate the rill erosion experiments carried out by *Elliot et al.* [1989] for five different textured soils. The infiltration parameters and the friction factor were calibrated to reproduce the flow discharges and the flow velocities measured by *Elliot et al.* [1989]. The calibration revealed the distinction between the rougher cohesive soils and the smoother noncohesive soils. The detachment parameters (K_r and τ_{soil}) were taken from the WEPP database. Four sediment transport capacity equations were evaluated against the observed data: the Yalin, the Low, the Govers USP and the Govers ESP formulae. The Govers USP formula gave the best results for the cohesive soils. However, none of the equations performed well for the noncohesive soils; the simulations stopped early. This highlights that the model possibly miss some physical processes in such conditions.

[46] The spatial erosion patterns implied by the first-order detachment-transport coupling model were also examined for three of the five soils tested. However, the results are only a demonstration of how the model operates and could not be verified since no experimental data on rill morphology are available. For the Barnes_ND soil, the sediment load was limited by the detachment rate over the whole rill. For the Bonifay soil, the sediment load was limited by the transport capacity at the upper reaches of the channel. For the Collamer soil, the sediment load was limited by the detachment rate near the upper end of the rill but the transport capacity controlled the sediment delivery in the lower part.

[47] The numerical experiments carried out in this study revealed the limits of PSEM_2D. In some cases the simulations did not reach the end. PSEM_2D accounts for morphological evolution as a result of erosion but it cannot handle rapidly changing hydraulic conditions because of very strong erosion. The two dimensional Saint Venant

equations cannot be used to reproduce the formation of deep rills.

Notation

- D_{fd_d} detachment/deposition rate of sediment from original soil by runoff, $\text{kg m}^{-2} \text{ s}^{-1}$.
- D_{fd_e} entrainment/deposition rate of sediment from the covering layer by runoff, $\text{kg m}^{-2} \text{ s}^{-1}$.
- D_s sediment diameter, m.
- D_{50} median diameter, m.
- f Darcy-Weisbach friction factor.
- Fr Froude number.
- g gravitational acceleration, m s^{-2} .
- h flow depth, m.
- h_f wetting front capillary pressure head, m.
- K_r flow erodibility parameter, s m^{-1} .
- K_s hydraulic conductivity at saturation, m s^{-1} .
- K_{SP} coefficient of efficiency of transport in the Low formula, $\text{s}^2 \text{ m}^{-1}$.
- K_t coefficient of efficiency of transport in the Yalin formula, $\text{s}^2 \text{ m}^{-1}$.
- q flow discharge per unit flow width in the flow direction, $\text{m}^2 \text{ s}^{-1}$.
- q_s sediment discharge per unit flow width, kg s^{-1} .
- Q_s sediment discharge, kg s^{-1} .
- Re Reynolds number.
- S_f friction slope.
- SP stream power, kg s^{-3} .
- T_c sediment transport capacity of the flow, $\text{kg m}^{-1} \text{ s}^{-1}$.
- \bar{V} depth-averaged flow velocity in the direction of the flow, m s^{-1} .
- Y dimensionless shear stress.
- Y_{cr} critical dimensionless shear stress.
- ϵ percentage of a grid cell covered by the covering layer.
- Φ degree of mixing of the sediment concentration within the flow depth.
- θ_i initial volumetric water content.
- θ_s saturation volumetric water content.
- ρ water density, kg m^{-3} .
- ρ_s sediment density, kg m^{-3} .

- τ flow shear stress in the flow direction, Pa.
 τ_c critical shear stress of the non-cohesive particles, Pa.
 τ_{soil} critical shear stress of the cohesive soil, Pa.

[48] **Acknowledgments.** The authors are grateful for the financial support provided by Institut de Recherche pour le Développement (IRD) and the French National Research Program on Hydrology (PNRH). The authors thank the two anonymous reviewers for providing constructive comments that have improved the clarity and quality of the paper. The authors also thank W. Elliot for the experimental data and for scientific discussion.

References

- Alonso, C. V., W. H. Neibling, and G. R. Foster (1981), Estimating sediment transport capacity in watershed modeling, *Trans. ASAE*, 24, 1211–1226.
- Bennett, J. P. (1974), Concepts of mathematical modeling of sediment yield, *Water Resour. Res.*, 10(3), 485–492.
- Davis, S. S., G. R. Foster, and L. F. Huggins (1983), Deposition of nonuniform sediment on concave slopes, *Trans. ASAE*, 26, 1057–1063.
- Elliot, W., A. Liebenow, J. Laflen, and K. Kohl (1989), A compendium of soil erodibility data from WEPP cropland soil field erodibility experiments 1987 and 1988, *NSERL Rep. 3*, Natl. Soil Erosion Res. Lab., Agric. Res. Serv., U.S. Dep. of Agric., West Lafayette, Indiana. (Available at <http://topsoil.nserl.purdue.edu/nserlweb/weppmain/comp/html>.)
- Esteves, M., X. Faucher, S. Galle, and M. Vauclin (2000), Overland flow and infiltration modelling for small plots during unsteady rain: Numerical results versus observed values, *J. Hydrol.*, 228(3), 265–282.
- Ferro, V. (1998), Evaluating overland flow sediment transport capacity, *Hydrol. Processes*, 12(12), 1895–1910.
- Foster, G. R. (1982), Modeling the erosion process, in *Hydrologic Modeling of Small Watersheds, ASAE Monogr.*, vol. 5, edited by C. Haan and D. Brakensiek, pp. 295–380, Am. Soc. of Agric. Eng., St. Joseph, Mich.
- Foster, G. R., and L. D. Meyer (1972), A closed-form soil erosion equation for upland areas, in *Sedimentation Symposium to Honor Prof. H. A. Einstein*, vol. 12, edited by H. W. Shen, pp. 12.1–12.19, Colo. State Univ., Fort Collins, Colo.
- Foster, G. R., R. A. Young, and W. H. Neibling (1985), Sediment composition for non-point source pollution analyses, *Trans. ASAE*, 28, 133–139.
- Foster, G. R., D. C. Flanagan, M. A. Nearing, L. J. Lane, L. M. Risse, and S. C. Finkner (1995), Hillslope erosion component, in *Water Erosion Prediction Project: Hillslope Profile and Watershed Model Documentation, USDA NSERL Rep. 10*, edited by D. C. Flanagan and M. Nearing, chap. 11, 11.1–11.12, Natl. Soil Erosion Res. Lab., Agric. Res. Serv., U.S. Dep. of Agric., West Lafayette, Indiana.
- Gimenez, R., and G. Govers (2002), Flow detachment by concentrated flow on smooth and irregular bed, *Soil Sci. Soc. Am. J.*, 66, 1475–1483.
- Gimenez, R., O. Planchon, N. Silvera, and G. Govers (2004), Longitudinal velocity patterns and bed morphology interactions in a rill, *Earth Surf. Processes Landforms*, 29, 105–114.
- Govers, G. (1992), Evaluation of transporting capacity formulae for overland flow, in *Overland Flow, Hydraulics and Erosion Mechanics*, edited by A. Parsons and A. Abrahams, 243–273, UCL Press, London.
- Govers, G., and G. Rauws (1986), Transporting capacity of overland flow on plane and on irregular beds, *Earth Surf. Processes Landforms*, 11, 515–524.
- Guy, B. T., R. P. Rudra, and W. T. Dickinson (1992), Process-oriented research on soil erosion and overland flow, in *Overland flow*, edited by A. J. Parsons and A. D. Abrahams, 225–242, UCL Press, London.
- Hairsine, P.-B., and C.-W. Rose (1992), Modeling water erosion due to overland flow using physical principles: 1. Sheet flow, *Water Resour. Res.*, 28(1), 237–243.
- Huang, C.-H., J. M. Bradford, and J. M. Laflen (1996), Evaluation of the detachment-transport coupling concept in the WEPP rill erosion equation, *Soil Sci. Soc. Am. J.*, 60, 734–739.
- Lei, T., M. Nearing, K. Haghighi, and V. F. Bralts (1998), Rill erosion and morphological evolution: A simulation model, *Water Resour. Res.*, 34(11), 3157–3168.
- Low, H. S. (1989), Effect of sediment density on bed-load transport, *J. Hydraul. Eng.*, 115, 124–138.
- Merten, G. H., M. A. Nearing, and A. L. O. Borges (2001), Effect of sediment load on soil detachment and deposition in rills, *Soil Sci. Soc. Am. J.*, 65, 861–868.
- Nearing, M. A., G. R. Foster, L. J. Lane, and S. C. Finkner (1989), A process-based soil erosion model for usda-water erosion prediction project technology, *Trans. ASAE*, 32, 1587–1593.
- Nearing, M. A., L. D. Norton, D. A. Bulgakov, G. A. Larionov, L. T. West, and K. M. Dontsova (1997), Hydraulics and erosion in eroding rills, *Water Resour. Res.*, 33(4), 865–876.
- Nord, G., and M. Esteves (2005), PSEM_2D: A physically based model of erosion processes at the plot scale, *Water Resour. Res.*, 41, W08407, doi:10.1029/2004WR003690.
- Polyakov, V. O., and M. A. Nearing (2003), Sediment transport in rill flow under deposition and detachment conditions, *Catena*, 51(1), 33–43.
- Polyakov, V. O., and M. A. Nearing (2004), Rare earth element oxides for tracing sediment movement, *Catena*, 55(3), 255–276.
- Rhoton, F. E., L. D. Meyer, and F. D. Whisler (1983), Densities of wet aggregates sediment from different textured soils, *Soil Sci. Soc. Am. J.*, 47, 576–578.
- Sharma, P. P., S. C. Gupta, and G. R. Foster (1993), Predicting soil detachment by raindrops, *Soil Sci. Soc. Am. J.*, 57, 674–680.
- Smart, G. M. (1984), Sediment transport formula for steep channels, *J. Hydraul. Eng.*, 110, 267–276.
- Walling, D. E. (1990), Linking the field to the river: Sediment delivery from agricultural land, in *Soil Erosion on Agricultural Land*, edited by I. F. J. Boardman and J. Dearing, pp. 129–152, John Wiley, Hoboken, N. J.
- Walling, D. E. (2005), Tracing suspended sediment sources in catchments and river systems, *Sci. Total Environ.*, 344, 159–184.
- Yalin, M. S. (1963), An expression for bed-load transportation, *Proc. Am. Soc. Civ. Eng.*, 89, 221–250.
- Yalin, M. S., and E. Karahan (1979), Incipient of sediment transport, *J. Hydraul. Div. Am. Soc. Civ. Eng.*, 105(11), 1433–1443.

M. Esteves, UMR 5564, Laboratoire d'Étude des Transferts en Hydrologie et Environnement, CNRS, INPG, IRD, UJF, BP 53, F-38041 Grenoble Cedex 9, France. (Michel.Esteves@hmg.inpg.fr)

G. Nord, UMR 1572, Laboratoire des Sciences du Climat et de l'Environnement, CNRS, CEA, UVSQ, Domaine du CNRS, F-91198 Gif sur Yvette Cedex, France. (guillaume.nord@lsce.cnrs-gif.fr)